

# Emergence and percolation of rigid domains during colloidal glass transition

Xiunan Yang<sup>+,1,2</sup> Hua Tong<sup>+,3</sup> Wei-Hua Wang<sup>\*,4,2</sup> and Ke Chen<sup>\*,1,2</sup>

<sup>1</sup>*Beijing National Laboratory for Condensed Matter Physics and Key Laboratory of Soft Matter Physics, Institute of Physics, Chinese Academy of Sciences, Beijing 100190, People's Republic of China*

<sup>2</sup>*University of Chinese Academy of Science, Beijing 100049, People's Republic of China*

<sup>3</sup>*Department of Fundamental Engineering, Institute of Industrial Science, University of Tokyo, 4-6-1 Komaba, Meguro-ku, Tokyo 153-8505, Japan*

<sup>4</sup>*Institute of Physics, Chinese Academy of Sciences, Beijing 100190, People's Republic of China*

(Dated: May 24, 2022)

Using video microscopy, we measure local spatial constraints in disordered binary colloidal samples, ranging from dilute fluids to jammed glasses, and probe their spatial and temporal correlations to local dynamics during the glass transition. We observe the emergence of significant correlations between constraints and local dynamics within the Lindemann criterion, which coincides with the onset of glassy dynamics in supercooled liquids. Rigid domains in fluids are identified based on local constraints, and demonstrate a percolation transition near glass transition, accompanied by the emergence of dynamical heterogeneities. Our results show that the spatial constraints instead of the geometry of amorphous structures is the key that connects the complex spatial-temporal correlations in disordered materials.

When a liquid solidifies, the motions of the molecules become mechanically constrained by the rigid structures in the materials. For crystals, the spatial distributions of the mechanical constraints faithfully reflect the symmetry of the underlying lattices, and the constraints experienced by individual atoms can be effectively described by simple geometric parameters such as lattice constants or coordination numbers. For glasses, however, such simple metrics generally fail to connect to the dynamical, thermodynamical or mechanical properties of the materials, due to the apparently disordered arrangements of atoms. Previous studies attempt to construct more complex geometric parameters to distinguish rigid regions from the more mobile fluid regions, using free volume [1], crystalline order parameter [2], and local five-fold symmetry [3–5]. Each of these parameters is effective for certain type of glassy systems, but none is universally applicable. Without a proper identifier for rigid or ordered regions in amorphous materials, how glasses acquire rigidity through glass transitions remains unsolved. On the other hand, if the degree of local constraints in glasses can be directly ascertained, its correlations to dynamics or other macroscopic properties of glasses may be established without the need for explicit information on the local geometry, which is usually system specific. Using the simplest measure for spatial constraints in glasses, recent simulations show that the shear modulus of glasses can be determined by the mean square displacements (MSDs) [6, 7].

In this Letter, we employ soft phonon modes [8–11] and particle positional variances to measure the local constraints in colloidal liquids and glasses. Temporal correlations between spatial constraints and local dynamics reveal the proper time scale to measure local structures in unjammed liquids. As the temperature decreases, the rise of rearranging barriers in supercooled liquids is observed,

indicating the formation of meta-stable rigid domains, which are identified by applying the Lindemann criterion. The onset of glassy dynamics is shown to coincide with the percolation of rigid domains in supercooled liquids, when the dynamical heterogeneity increases sharply. Dynamical heterogeneity decreases when the system becomes overwhelmingly rigid. Our results suggest that the glass transition is the growth of structural order in liquids represented by the rigid domains identified by local spatial constraints, instead of geometric or topological configurations.

The samples consist of binary mixtures of poly-N-isopropylacrylamide (PNIPAM) particles [12, 13] hermetically sealed between two coverslips, forming a monolayer of disordered packing. To avoid crystallization, the diameter ratio between large and small particles is chosen to be 1:1.4, with the number ratio close to 1. The PNIPAM particles are thermo-sensitive which allows the in-situ tuning of the packing fractions using an objective heater (BiOptechs). To cover a wide range of packing fractions, two groups of samples are separately prepared. The packing fractions are between 0.890 to 0.850 (jammed solids) for the first group, and between 0.56 and 0.84 (unjammed liquids) for the second group. Before data acquisition, the samples are equilibrated on microscope stage for 3 hours. The particle configurations are recorded by digital video microscopy at 30 to 110 frames/s, and the particle trajectories are extracted by particle-tracking techniques [14]. For jammed samples, the phonon modes are extracted using the covariance matrix analysis [9, 15–17].

We first investigate the correlations between soft modes and local dynamics in jammed colloidal glasses. We employ a soft mode parameter  $\Psi$  for individual particles, proposed by Tong and Xu [18] based on equipartition hypothesis. For particle  $i$ ,  $\Psi_i^{2N} = \sum_{j=1}^{2N} \frac{1}{\omega_j^2} |\vec{e}_{j,i}|^2$ , where  $\omega_j$  is the vibrational frequency of mode  $j$  and  $\vec{e}_{j,i}$

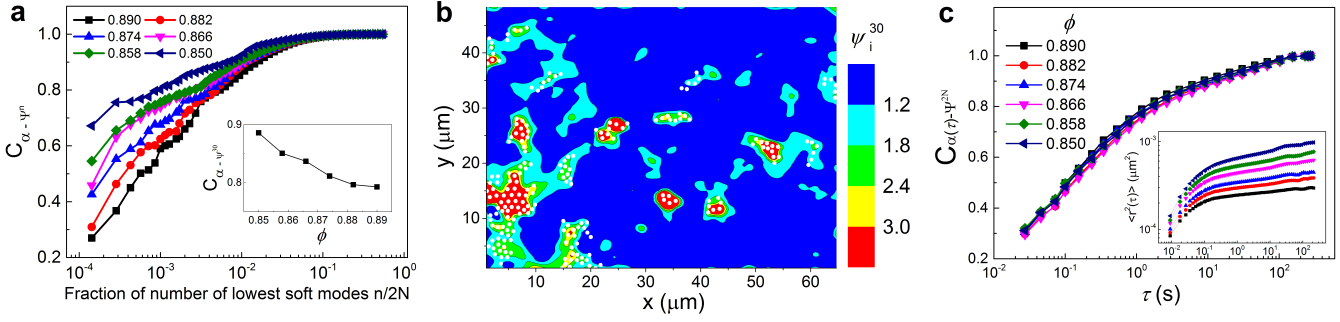


Figure 1. **Correlation between soft modes and positional variances in jammed packings.** **a**, Correlation between  $\alpha_i$  and  $\Psi_i^n$  as a function of the fraction of the lowest frequency modes  $n/2N$  included in  $\Psi_i^n$  at different packing fractions. Inset: correlations between  $\alpha$  and  $\Psi^{30}$  at different packing fractions. The noise level is about 0.02. **b**, Real space distribution of cooperatively rearranging regions (white dots) and  $\Psi^{30}$  at  $\phi = 0.850$  (colored contours), normalized by the average value. **c**, Rank correlations between  $\Psi_i^{2N}$  and  $\alpha_i(\tau)$  as a function of  $\tau$  for different packing fractions. The noise level is about 0.02. Inset: MSDs at different  $\phi$ .

is the polarization vector of particle  $i$  in mode  $j$ ,  $N$  is the number of particles in a two-dimensional glass.  $\Psi_i^{2N}$  is biased toward the lower frequency modes, as the contributions from high frequency modes to  $\Psi_i^{2N}$  diminish rapidly with frequency.  $\Psi_i^{2N}$  removes the ambiguities in soft modes selections, and can be proven to be equivalent to the positional variance of particle  $i$ ,  $\alpha_i = \langle [\vec{r}_i(t) - \vec{r}_i(t)]^2 \rangle_t$  (See supplementary for derivations [17]).

Figure 1a plots the Spearman's rank correlation between  $\Psi_i^n$  and  $\alpha_i$  as a function of the fraction of the lowest frequency modes  $n/2N$  included in jammed colloidal glasses. The correlation to local dynamics comes predominantly from the lowest frequency modes, as the bottom 0.5% of modes ( $\sim 30$  for our system) achieve a correlation over 0.8. Figure 1b shows the spatial distribution of cooperatively rearranging regions (CRRs) composed of the top 10% fastest particles (white circles) [19] and  $\Psi_i^{30}$  (colored contours). It is clear that regions with higher concentration of soft modes are spatially correlated with fast local dynamics. The inset of Figure 1a shows the correlation between  $\Psi_i^{30}$  and  $\alpha_i$  at different packing fractions. The high correlation between  $\Psi_i^{30}$  and  $\alpha_i$  suggests that in jammed solids where topological relaxations are rare on the time scale of the experiment, the local dynamics are almost entirely determined by a small number of soft modes.

In jammed glasses, soft modes can be accounted for by short-time fluctuations of particle positions. Figure 1c plots the correlation between  $\alpha_i(\tau)$  and  $\Psi_i^{2N}$  as a function of the time window  $\tau$  in which  $\alpha_i$  is measured. The correlation increases rapidly for small  $\tau$  values and reaches  $\sim 0.8$  at  $\sim 1$ s, within the  $\beta$ -relaxation time scale ( $\sim 10$ s) defined by the middle of the plateau in the log-log plot of the mean square displacements (Figure 1c, inset) [20]. The high correlations between short-time  $\alpha_i(\tau)$  and  $\Psi_i^{2N}$  suggest that the local structures can be adequately explored at relatively short periods of time. Further in-

creasing of  $\tau$  only slightly improves the correlation to soft modes. For comparison, it requires more than 1000s of video microscopy measurements to properly extract the vibrational modes from the same jammed colloidal samples using covariance matrix analysis [16].  $\alpha_i(\tau)$  measured in  $\beta$ -relaxation time scale also demonstrates comparable predicting power to soft spots for structural rearrangements in jammed colloidal glasses [17]. Thus short-time particle positional variance can be employed as an effective soft mode parameter in colloidal systems below jamming [21], where direct measurements of spatial distribution of soft modes are difficult.

We now apply  $\alpha_i(\tau)$  in unjammed colloidal liquids to measure local mechanical constraints. The MSDs of the unjammed samples are plotted in Figure 2a. We investigate the temporal correlations between  $\alpha_i(\tau)$  and local dynamics measured by non-affine displacement  $D_{\min}^2(\Delta t)$  [22, 23] after the variances are measured.  $D^2(t_1, t_2) = \sum_n \sum_i [r_{n,t_2}^i - r_{0,t_2}^i - \sum_j (\delta_{ij} + \varepsilon_{ij}) \times (r_{n,t_1}^j - r_{0,t_1}^j)]^2$ , where  $r_{n,t}^i$  is the  $i$ th ( $x$  or  $y$ ) component of the position of the  $n$ th particle at time  $t$ , and the  $\delta_{ij} + \varepsilon_{ij}$  that minimize  $D^2$  are calculated based on  $r_{n,t}^i$ . Correlations between  $\alpha_i(\tau)$  and  $D_{\min}^2(\Delta t)$  depend on both the window  $\tau$  in which structural information is collected, and the timescale of the dynamics after  $\alpha_i$  is measured,  $\Delta t$ . We choose the  $\tau = \tau_{\max}$  that yields the highest correlations to  $D_{\min}^2$  [17].  $\tau_{\max}$  is thus the proper time scale to identify structures that have the highest predictability for dynamics in liquids; and it naturally emerges from correlation measurements. For observation window shorter than  $\tau_{\max}$ , insufficient structural information is collected, and for much longer time windows, relevant information will eventually be lost in structural relaxations. In our experiments,  $\tau_{\max}$  is found to be in the vicinity of  $\beta$ -relaxation time  $\tau_\beta$  [17], consistent with our results from jammed solids. The  $\beta$ -relaxation time and  $\alpha$ -relaxation

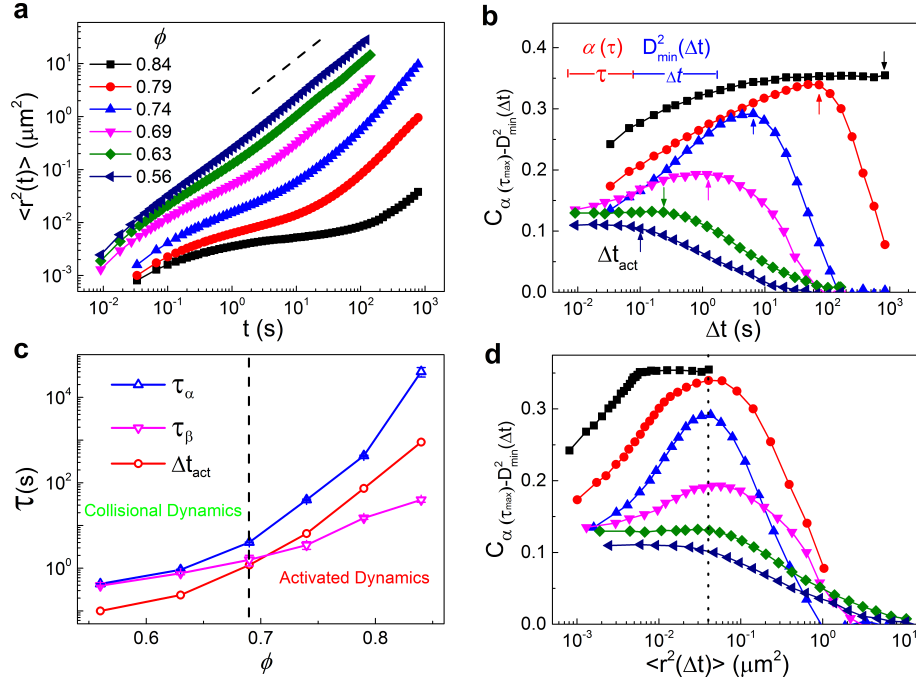


Figure 2. **Structure-dynamics correlation during glass transition.** **a**, Measured mean square displacements at different packing fractions. Dashed line indicates free diffusive motions. **b**, Spearman's rank correlation between  $\alpha_i(\tau_{\max})$  and  $D_{\min}^2(\Delta t)$  as a function of  $\Delta t$ . The vertical arrows indicate the  $\Delta t_{\text{act}}$  when the correlations start to decay. Inset: the time sequence for measuring  $\alpha(\tau)$  and  $D_{\min}^2(\Delta t)$ . **c**,  $\phi$  dependence of the activation time  $\Delta t_{\text{act}}$ , and the  $\alpha$  and  $\beta$  relaxation time. The dashed line indicates the onset of glassy dynamics. **d**, MSDs dependence of correlation  $C_{\alpha_i(\tau_{\max})-D_{\min}^2(\Delta t)}$  for each packing fraction. Vertical dashed line indicates the Lindemann criterion. The noise level is about 0.02.

time of the samples are extracted by fitting the intermediate scattering function with a two-step stretched exponential function (the Kohlrausch-Williams-Watts function) [17, 24, 25].

Figure 2b plots the correlation between  $\alpha_i(\tau_{\max})$  and  $D_{\min}^2(\Delta t)$  as a function of  $\Delta t$ . The correlations are averaged over all available trajectories. At low packing fractions, the correlation between  $\alpha_i(\tau_{\max})$  and local dynamics is low, and decays almost immediately after the  $\alpha_i(\tau_{\max})$  is measured. This short memory in dynamics reflects a nearly flat potential energy landscape where structural relaxations are facilitated by free diffusion and collisions between particles. The energy landscape becomes more rugged as the packing fraction increases, and an activation mechanism begins to emerge [26]. At higher packing fractions, the correlation between  $\alpha_i(\tau_{\max})$  and  $D_{\min}^2$  first increases with  $\Delta t$  then decreases after reaching a peak value at  $\Delta t_{\text{act}}$ . This delayed correlation peak between local constraints and dynamics signifies the emergence of rearranging barriers, hence meta-stable rigid structures in liquids, with  $\Delta t_{\text{act}}$  being the average time required for thermal fluctuations to overcome the barriers for structural relaxations. When the packing fraction is further increased, this activation mechanism becomes more dominant, with higher peak correlation values.

The rise of the relaxation barriers coincides with the separation of  $\alpha$ - and  $\beta$ -relaxation time scales in liquids [27]. Figure 2c plots the measured  $\tau_{\alpha}$ ,  $\tau_{\beta}$  and  $\Delta t_{\text{act}}$  in unjammed colloidal samples. Below  $\phi = 0.69$ ,  $\Delta t_{\text{act}}$  is short, and the  $\tau_{\alpha}$  and  $\tau_{\beta}$  are close. Without obvious peaks,  $\Delta t_{\text{act}}$  is chosen to be the point where the correlation between  $\alpha_i(\tau)$  and  $D_{\min}^2$  starts to decay, as indicated by vertical arrows in Figure 2b. Around  $\phi = 0.69$  where a delayed correlation peak appears, the  $\alpha$ - and  $\beta$ -relaxation times begin to separate.  $\Delta t_{\text{act}}$  becomes significantly larger than  $\tau_{\beta}$  when the packing fraction is further increased. As the  $\alpha_i(\tau)$  is measured on the time scale of  $\tau_{\beta}$ , a  $\Delta t_{\text{act}}$  greater than  $\tau_{\beta}$  allows the prediction of long-time dynamics with short-time structural information, as the meta-stable structures persist much longer than the average relaxation time of a single particle. The gap between  $\Delta t_{\text{act}}$  and  $\tau_{\beta}$  widens with the packing fraction, indicating increased stability of the meta-stable structures.

Temporally, local dynamics in liquids begin to decouple from earlier structures after  $\Delta t_{\text{act}}$  which increases rapidly with the packing fraction. An interesting question is that spatially how much the system configuration has evolved when the dynamics begin to de-correlate from an earlier structure. In Figure 2d, we replot the  $C_{\alpha_i-D_{\min}^2}$  as

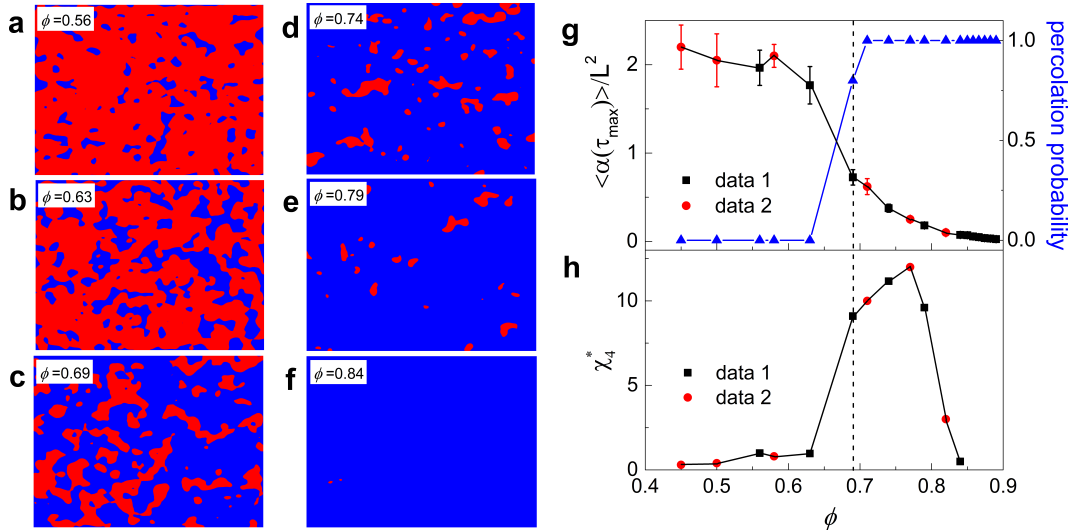


**Figure 3. Structure evolution during glass transition.** **a-f**, Spatial distribution of  $\alpha_i(\tau_{\max})$  at different packing fractions, binarized by the Lindemann criterion. Red colors are fluid regions with  $\alpha_i(\tau_{\max})$  larger than the Lindemann criterion; blue colors are rigid regions with  $\alpha_i(\tau_{\max})$  below the Lindemann criterion. **g**, Average  $\alpha_i(\tau_{\max})$  and the percolation of rigid regions during glass transition. Left axis: average  $\alpha_i(\tau_{\max})$  normalized by Lindemann criterion, as a function of  $\phi$ . The dashed line indicates the onset of glassy dynamics shown in Figure 3c. The black squares (data 1) are measured from the same dataset as in Figure 1 and Figure 2. To extend the range of the plot, we include measurements from an additional dataset (data 2, red circles). Error bars represent standard deviations. Right axis: The probability of rigid regions percolating the field of view (blue triangles). The probability is calculated as the fraction of the configurations with rigid regions percolating the field of view in all measured configurations. **h**, Peak value of dynamical susceptibility,  $\chi_4^*$  as a function of  $\phi$ .

a function of system MSDs. For all the packing fractions, the correlation begins to decay around 20% of the particle diameter (dashed line), close to the Lindemann criterion for the melting of crystals [28], despite orders of magnitude differences in relaxation time scales between these liquid samples. This universal length scale shows that in unjammed liquids, the structure-dynamics correlation is determined by the spatial distance instead of the temporal distance to earlier configurations. As long as the average configurational changes are below the Lindemann threshold, the system can resist external perturbations thus exhibits rigidity, regardless of the actual time the system takes to reach this threshold (or whether this threshold is reachable at all in a reasonable time at even higher packing fractions).  $\Delta t_{\text{act}}$  is the average time for the structure of the system to evolve beyond the Lindemann threshold. It is not clear, from our experiments, whether or not  $\Delta t_{\text{act}}$  will diverge at a finite packing fraction. Thus the Lindemann criterion can be generalized from the melting of crystals to the transition between rigid and fluid phases in amorphous materials [29, 30], where the demarcation between solid and fluid may also depend on the observation time.

Using the time window of  $\tau_{\max}$ , we identify rigid regions in unjammed samples whose  $\alpha_i(\tau_{\max})$  are below the Lindemann criterion, and fluid regions with higher  $\alpha_i(\tau_{\max})$  during the glass transition. Figure 3a-f plot

the snapshots of spatial distribution of  $\alpha_i(\tau_{\max})$  at different packing fractions, binarized by the Lindemann criterion. At low packing fractions, the system is mostly fluid-like (red color) with small pockets of rigid regions (blue color). The rigid regions grow with the packing fraction and begin to percolate the system around  $\phi = 0.69$  until complete solidification near the jamming point. The percolation probability of rigid regions and the averaged  $\alpha_i(\tau_{\max})$  of the system shows a sharp transition around  $\phi = 0.69$ , as plotted in Figure 3g.

The growth and percolation of the rigid regions in cooling liquids provide a microscopic origin for the onset of glassy dynamics shown in Figure 2c and dynamical heterogeneity. At low packing fractions (high temperatures), rigid structures are created and destroyed by thermal fluctuations, with relatively small sizes and short life time. The size and the fraction of rigid regions both increase as the samples are further cooled. At a critical packing fraction ( $\phi = 0.69$  in our experiments), the rigid regions become connected and percolate the system [31, 32], which greatly increases the stability of the whole system. The activated dynamics of the spanning rigid regions is much slower than the dynamics of the fluid regions governed by particle diffusions, hence the separation of the  $\tau_\alpha$ ,  $\tau_\beta$  time scales. Dynamical heterogeneity naturally emerges from the competition between the different relaxation dynamics of the fluid regions and the

percolating rigid regions [33]. The peak of the dynamical susceptibility  $\chi_4^*$  first increases around  $\phi = 0.69$  and then decreases near the jamming point ( $\phi_j \sim 0.85$ ) when the whole system becomes homogeneously rigid [34], as plotted in Figure 3h (for the measurements of  $\chi_4^*$ , see the supplementary materials [17, 35, 36]). We note that the percolation of rigid regions depends on the observation time window  $\tau$  in  $\alpha_i(\tau)$ . For a observation window different from  $\tau_{\max}$ , the percolation of rigid regions will occur at a packing fraction before or after the onset of glassy dynamics, which further proves that  $\tau_{\max}$  is the proper time scale to characterize structures in liquids, and is the correct scaling factor to compare the structures of liquids or glasses of different temperatures.

In summary, by measuring the local constraints in colloidal liquids and glasses, we directly observe the emergence and growth of structure-dynamics correlations in supercooled liquids. Based on the measured correlations, we extract the proper time and length scales to identify structures that are most relevant to glassy dynamics. The glass transition is then shown to be the growth and percolation of the rigid regions in supercooled liquids, which could be employed to explain the slowing-down and the dynamical heterogeneity [33, 37]. Our results are strong evidence that local constraints are a more useful parameter to connect structure to dynamics in glassy systems than purely geometric or topological metrics. However, this discovery does not render the geometric structures irrelevant in the physics of glasses. It is obvious that the spatial constraints in glasses depend sensitively on local configurations, although specific dependence may vary greatly from system to system. They are simply different ways to describe the same collection of interacting atoms in a material. It is only through the lens of the constraints can the correlations between structures and dynamics in disordered systems be clearly demonstrated. In addition, local constraints naturally include multi-body effects of amorphous structures that are difficult to quantify from analyzing the geometric structures alone. A direct link between conventional geometric structures and glassy dynamics may be established by searching for local and non-local configurations that contribute the most to local constraints in glassy materials [38].

---

<sup>+</sup> X.Y., and H.T. contributed equally to this work.

<sup>\*</sup> kechen@iphy.ac.cn

<sup>\*</sup> whw@iphy.ac.cn

- [1] F. Spaepen, A microscopic mechanism for steady state inhomogeneous flow in metallic glasses. *Acta Metall.* **25**, 407 (1977).
- [2] H. Tanaka, T. Kawasaki, H. Shintani, and K. Watanabe,

- Critical-like behaviour of glass-forming liquids. *Nature Mater.* **9**, 324 (2010).
- [3] H. W. Sheng, W. K. Luo, F. M. Alamgir, J. M. Bai, and E. Ma, Atomic packing and short-to-medium-range order in metallic glasses. *Nature* **439**, 419 (2006).
- [4] K. F. Kelton *et al.* First X-Ray scattering studies on electrostatically levitated metallic liquids: demonstrated influence of local icosahedral order on the nucleation barrier. *Phys. Rev. Lett.* **90**, 195504 (2003).
- [5] Y.-C. Hu, F.-X. Li, M.-Z. Li, H.-Y. Bai, and W.-H. Wang, Five-fold symmetry as indicator of dynamic arrest in metallic glass-forming liquids. *Nat. Commun.* **6**, 8310 (2015).
- [6] S. Saw and P. Harrowell, Rigidity in Condensed Matter and Its Origin in Configurational Constraint. *Phys. Rev. Lett.* **116**, 137801 (2016).
- [7] J. Ding *et al.* Universal structural parameter to quantitatively predict metallic glass properties. *Nat. Commun.* **7**, 13733 (2016).
- [8] A. Widmer-Cooper, H. Perry, P. Harrowell, and D. R. Reichman, Irreversible reorganization in a supercooled liquid originates from localized soft modes. *Nature Phys.* **4**, 711 (2008).
- [9] K. Chen *et al.* Measurement of Correlations between Low-Frequency Vibrational Modes and Particle Rearrangements in Quasi-Two-Dimensional Colloidal Glasses. *Phys. Rev. Lett.* **107**, 108301 (2011).
- [10] M. L. Manning and A. J. Liu, Vibrational Modes Identify Soft Spots in a Sheared Disordered Packing. *Phys. Rev. Lett.* **107**, 108302 (2011).
- [11] N. Xu, V. Vitelli, A. J. Liu, and S. R. Nagel, Anharmonic and quasi-localized vibrations in jammed solids - Modes for mechanical failure. *Europhys. Lett.* **90**, 56001 (2010).
- [12] P. J. Yunker *et al.* Physics in ordered and disordered colloidal matter composed of poly(N-isopropyl acrylamide) microgel particles. *Rep. Prog. Phys.* **77**, 056601 (2014).
- [13] K. Chen *et al.* Phonons in two-dimensional soft colloidal crystals. *Phys. Rev. E* **88**, 022315 (2013).
- [14] J. C. Crocker and D. G. Grier, Methods of digital video microscopy for colloidal studies *J. Colloid Interface Sci.* **179**, 298 (1996).
- [15] S. Henkes, C. Brito, and O. Dauchot, Extracting vibrational modes from fluctuations: a pedagogical discussion. *Soft Matter* **8**, 6092 (2012).
- [16] K. Chen *et al.* Low-Frequency Vibrations of Soft Colloidal Glasses. *Phys. Rev. Lett.* **105**, 025501 (2010).
- [17] See Supplemental Material at <http://link.aps.org/supplemental/> for a discussion of additional experimental details.
- [18] H. Tong and N. Xu, Order parameter for structural heterogeneity in disordered solids. *Phys. Rev. E* **90**, 010401 (2014).
- [19] G. Adam and J. H. Gibbs, On the Temperature Dependence of Cooperative Relaxation Properties in Glass-Forming Liquids. *J. Chem. Phys.* **43**, 139 (1965).
- [20] A. Widmer-Cooper and P. Harrowell, Predicting the Long-Time Dynamic Heterogeneity in a Supercooled Liquid on the Basis of Short-Time Heterogeneities. *Phys. Rev. Lett.* **96**, 185701 (2006).
- [21] R. L. Jack, A. J. Dunleavy, and C. P. Royall, Information-Theoretic Measurements of Coupling between Structure and Dynamics in Glass Formers. *Phys. Rev. Lett.* **113**, 095703 (2014).
- [22] X. Yang, R. Liu, M. Yang, W.-H. Wang, and K.

- Chen, Structures of local rearrangements in soft colloidal glasses. *Phys. Rev. Lett.* **116**, 238003 (2016).
- [23] M. L. Falk, and J. S. Langer, Dynamics of viscoplastic deformation in amorphous solids. *Phys. Rev. E* **57**, 7192 (1998).
  - [24] J. Mattsson *et al.* Soft colloids make strong glasses. *Nature* **462**, 83(2009).
  - [25] T. Kawasaki and H. Tanaka, Structural evolution in the aging process of supercooled colloidal liquids. *Phys. Rev. E* **89**, 062315 (2014).
  - [26] V. Lubchenko, Theory of the structural glass transition: a pedagogical review. *Advances in Physics* **64**, 283 (2015).
  - [27] P. G. Debenedetti and F. H. Stillinger, Supercooled liquids and the glass transition. *Nature* **410**, 259 (2001).
  - [28] F. A. Lindemann, The calculation of molecular Eigenfrequencies. *Phys. Z.* **11**, 609 (1910).
  - [29] H. B. Yu, R. Richert, R. Maaß, and K. Samwer, Unified Criterion for Temperature-Induced and Strain-Driven Glass Transitions in Metallic Glass. *Phys. Rev. Lett.* **115**, 135701 (2015).
  - [30] X. Xia and P. G. Wolynes, Fragilities of liquids predicted from the random first order transition theory of glasses. *Proc. Natl. Acad. Sci. U.S.A.* **97**, 2990 (2000).
  - [31] M. H. Cohen and G. S. Grest, Liquid-glass transition, a free-volume approach. *Phys. Rev. B* **20**, 1077 (1979).
  - [32] D. J. Jacobs and M. F. Thorpe, Generic Rigidity Percolation: The Pebble Game. *Phys. Rev. Lett.* **75**, 4051 (1995).
  - [33] D. Long, and F. Lequeux, Heterogeneous dynamics at the glass transition in van der Waals liquids, in the bulk and in thin films. *Eur. Phys. J. E* **4**, 371 (2001).
  - [34] P. Ballesta, A. Duri, and L. Cipelletti, Unexpected drop of dynamical heterogeneities in colloidal suspensions approaching the jamming transition. *Nature Phys.* **4**, 550 (2008).
  - [35] R. Candelier, O. Dauchot, and G. Biroli, Building Blocks of Dynamical Heterogeneities in Dense Granular Media. *Phys. Rev. Lett.* **102**, 088001 (2009).
  - [36] Z. Zhang, P. J. Yunker, P. Habdas, and A. G. Yodh, Cooperative Rearrangement Regions and Dynamical Heterogeneities in Colloidal Glasses with Attractive Versus Repulsive Interactions. *Phys. Rev. Lett.* **107**, 208303 (2011).
  - [37] G. Biroli, J.-P. Bouchaud, K. Miyazaki, and D. R. Reichman, Inhomogeneous Mode-Coupling Theory and Growing Dynamic Length in Supercooled Liquids. *Phys. Rev. Lett.* **97**, 195701 (2006).
  - [38] S. S. Schoenholz, E. D. Cubuk, D. M. Sussman, E. Kaxiras, and A. J. Liu, A structural approach to relaxation in glassy liquids. *Nature Phys.* **12**, 469 (2016).

**Acknowledgements** We thank Walter Kob, Peter Harrowell, Rui Liu, Mingcheng Yang, Chenhong Wang, and Maozhi Li for helpful discussions. This work was supported by the MOST 973 Program (No. 2015CB856800). K. C. also acknowledges the support from the NSFC (No. 11474327).